

Entanglement in XYZ model on a spin-star system: Anisotropy vs. field-induced dynamics

Jithin G. Krishnan, Harikrishnan K. J., and Amit Kumar Pal
Department of Physics, Indian Institute of Technology Palakkad, Palakkad 678 623, India
(Dated: August 1, 2023)

We consider a star-network of $n = n_0 + n_p$ spin- $\frac{1}{2}$ particles, where interaction between n_0 central spins and n_p peripheral spins are of the XYZ-type. In the limit $n_0/n_p \ll 1$, we show that for odd n , the ground state is doubly degenerate, while for even n , the energy gap becomes negligible when n is large, inducing an *effective* double degeneracy. In the same limit, we show that for vanishing xy -anisotropy γ , bipartite entanglement on the peripheral spins computed using either a partial trace-based, or a measurement-based approach exhibits a logarithmic growth with n_p , where the sizes of the partitions are typically $\sim n_p/2$. This feature disappears for $\gamma \neq 0$, which we refer to as the *anisotropy effect*. Interestingly, when the system is taken out of equilibrium by the introduction of a magnetic field of constant strength on all spins, the time-averaged bipartite entanglement on the periphery at the long-time limit exhibits a logarithmic growth with n_p irrespective of the value of γ . We further study the $n_0/n_p \gg 1$ and $n_0/n_p \rightarrow 1$ limits of the model, and show that the behaviour of bipartite peripheral entanglement is qualitatively different from that of the $n_0/n_p \ll 1$ limit.

I. INTRODUCTION

Entangled quantum states [1] have been shown to be a key resource for several quantum technological applications including quantum communication [2], quantum cryptography [3], quantum simulation [4], quantum metrology [5], measurement-based quantum computation [6], and quantum algorithms [7]. Being sources of entangled states, quantum many-body systems [8] have been identified as candidate systems for implementing these applications. The last two decades have also witnessed the laboratory realization of quantum many-body Hamiltonians leading to quantum states possessing bipartite and multipartite entanglement using trapped ions [9], nuclear magnetic resonance systems [10], ultra-cold atoms and optical lattices [11], and solid-state systems [12]. This has made testing the theoretically predicted entanglement properties of these systems possible. From this motivation, interface of quantum information theory and quantum many-body systems has emerged as a vibrant field of research advancing along two complementary directions. On one hand, quantum technological applications have been implemented using quantum many-body systems, eg. quantum state transfer through spin chains [13] and one-way quantum computation [6] using cluster states [14]. On the other hand, quantum information-theoretic concepts have been extensively used to probe quantum many-body systems [8], leading to the introduction of projected entangled pair states [15], and multiscale entanglement renormalization ansatz [16].

Among the variety of quantum many-body systems, interacting quantum spin models [8] have attracted bulk of the attention due to their natural representation of multi-qubit or multi-qudit systems pertinent to quantum protocols. Although one- and two-dimensional regular lattices have primarily been in focus [8], achievement of control over the connection between any two qubits in an array realized in different substrates [17] have also given rise to studies on quantum spin systems having a lattice structure modelled for specific purposes. Prime examples along this line of studies are (a) a star network of spins [18], where a number of *central spins* are surrounded by a number of *periph-*

eral spins such that each of the central spin interacts with all of the peripheral spins (see Fig. 1 for examples with one and two central spin(s)), and (b) a star-chain network of spins, where a number of spin-chains have a common boundary spin [19]. While such a network was originally envisioned for achieving control over entanglement through one, or a group of *preferred* (central) spins [18], they have also been used as switch in quantum networks [20], in quantum state transfer and cloning [21], in magnetic resonance imaging [22], in studying measurement uncertainty [23], and to implement quantum heat engines [24], refrigerators [25], and quantum batteries [26]. The static and dynamical properties of entanglement [18, 27, 28] in a star network of spins have also been extensively explored, along with the quantum correlations not belonging to the entanglement-separability paradigm [28, 29] (cf. [30]).

In this paper, we consider a star-network of $n = n_0 + n_p$ spins with n_0 central and n_p peripheral spins, where each central (peripheral) spin interacts with each peripheral (central) spin via a fully anisotropic XYZ interaction [31]. We consider three limits of the model – the *large periphery limit* given by $n_0/n_p \ll 1$, the *large center limit* given by $n_0/n_p \gg 1$, and the *competing center limit*, represented by $n_0/n_p \rightarrow 1$. In the large periphery limit, for non-zero values of the xy - and the z -anisotropy parameters, we investigate the structure of the ground state of the system. We show that for odd n , the ground states are doubly degenerate for all values of the anisotropy parameters. However, for even n , there is a finite energy gap between the ground and the first excited states for low and moderately high n . This energy gap decreases as $\exp(-bn_p^m)$ for $\gamma = 0$, and as bn_p^{-m} for $\gamma \neq 0$ with increasing n_p , and the ground state becomes *effectively* doubly degenerate with a negligible energy gap once a *critical size* n_p^c of the periphery (and hence, a critical size n_c of the system) is achieved.

We next investigate the interplay of the *bipartite entanglement* over the peripheral spins and the size of the partitions in the zero-temperature and large periphery limits of the system. We take two separate approaches for quantifying bipartite entanglement in the periphery. One is the partial trace-based approach, where the central spins are traced out of the state of the system, leading to a mixed state on the periph-

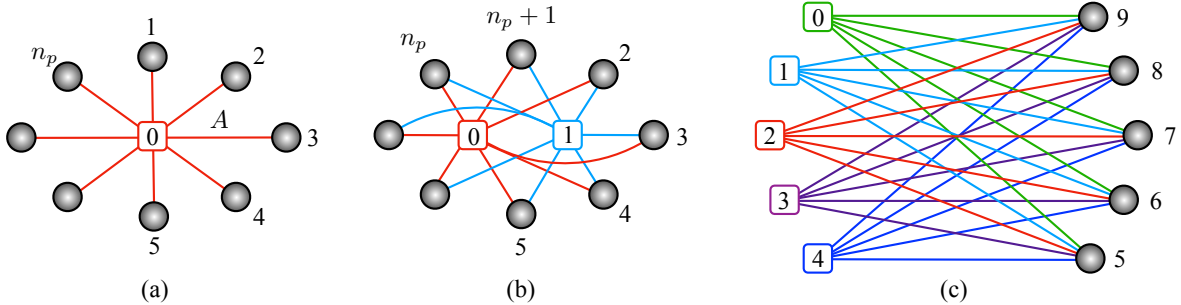


FIG. 1. (Color online.) Star networks of $n = n_0 + n_p$ spin- $\frac{1}{2}$ particles with (a) $n_0 = 1$ and (b) $n_0 = 2$, where peripheral spins are represented by shaded circles. As n_p increases, the large periphery limit $n_0/n_p \ll 1$ is achieved, while an interchange of the central spins with the peripheral spins (i.e., an interchange between n_0 and n_p) provides the limit $n_0/n_p \gg 1$. The equal periphery limit of the system with $n_0/n_p = 1$ is demonstrated with $n_0 = n_p = 5$ in (c). In these star networks, each spin in the periphery interacts with each of the central spin with XYZ interaction.

eral spins which can be used to compute a bipartite entanglement measure over a pre-fixed bipartition of the peripheral spins [1]. The other avenue is to *localize* [32–35] non-zero average bipartite entanglement on the peripheral spins by performing a judiciously chosen projection measurement on the central spins. For both cases, we show that the bipartite entanglement over the equal bipartition of the peripheral spins exhibits a growth as $\log_2 n_p$ with the periphery-size when the system has no xy -anisotropy (cf. [36] for a similar finding in the Lipkin-Meshkov-Glick (LMG) model), while for non-zero xy -anisotropy, this feature is absent. We refer to this as the *anisotropy effect*. Moreover, for a fixed system-size n with a partition-size n' , both types of bipartite entanglement varies as $a [1 - \exp(-b(n')^m)]$.

Next, we consider taking the $n_0/n_p \ll 1$ limit of the system out of equilibrium by turning on a magnetic field of constant strength on all spins. As the system evolves, we calculate the bipartite entanglement from both approaches as a function of time at different points in the parameter space of the xy - and z -anisotropy parameters. The time-averaged bipartite entanglement corresponding to both approaches in the long-time limit are shown to have a logarithmic growth with n_p for all values of the xy -anisotropy parameter, implying a negation of the anisotropy effect due to the field-induced dynamics. Also, similar to the static scenario, both types of average bipartite entanglement varies as $a [1 - \exp(-b(n')^m)]$ for a fixed n_p . We further consider the $n_0/n_p \gg 1$ and $n_0/n_p \rightarrow 1$ limits of the spin-star system, and find that the behaviours of bipartite peripheral entanglement in these limits are qualitatively different from the same for the $n_0/n_p \ll 1$ limit. In the case of $n_0/n_p \gg 1$, the bipartite peripheral entanglement decreases monotonically with increasing n_0 as $\sim bn_0^{-m}$, and vanishes asymptotically, while n_p is kept fixed. For $n_0/n_p \rightarrow 1$, the bipartite peripheral entanglement saturates with n_p .

The rest of the paper is organized as follows. In Sec. II, we introduce the XYZ model on the spin-star system, and provide brief definitions of the partial trace-based and measurement-based approaches for quantifying bipartite entanglement on the peripheral spins. In Sec. III A, we dis-

cuss the diagonalization of the system-Hamiltonian in the $n_0/n_p \ll 1$ limit, and explain the degeneracy and effective degeneracy of the ground state of the system for odd and even system sizes in Sec. III B. The static properties of peripheral bipartite entanglement in the large periphery limit of the system is discussed in Sec. III C, while the features of the dynamics of bipartite entanglement in the periphery due to the introduction of a magnetic field of constant magnitude is explored in Sec. III D. The limits $n_0/n_p \gg 1$ and $n_0/n_p \rightarrow 1$ are discussed in Sec. III E and Sec. IV respectively. Sec. V contains the concluding remarks and outlook.

II. DEFINITIONS

In this section, we set notations for describing the system, and present the necessary details for partial trace-based and measurement-based entanglement computed in the star network of spins.

A. Star network of spins

We consider a star-network [18, 20–29] of $n = n_0 + n_p$ spin- $1/2$ particles, where n_0 central spins are surrounded by n_p peripheral spins such that each of the central spin interacts with all of the peripheral spins, but there is no interaction among the central spins and the peripheral spins themselves. Without any loss in generality, we label the central spins as $0, 1, 2, \dots, n_0 - 1$, and the n_p peripheral spins as $n_0, n_0 + 1, n_0 + 2, \dots, n_0 + n_p - 1$. We consider three limits of the model,

- (a) the *large periphery limit*, $n_0/n_p \ll 1$, where the size of the periphery is far larger than the size of the center,
- (b) the *large center limit*, $n_0/n_p \gg 1$, where the central spins outnumber the peripheral spins by a large number, and

- (c) the *competing center limit*, $n_0/n_p \rightarrow 1$, where the number of central spins is comparable to the number of peripheral spins.

See Fig. 1 for pictorial representations of these limits of the system. We assume each of the central spins j interacting with all of the peripheral spins via the interaction Hamiltonian [31]

$$H_s = K \sum_{i=0}^{n_0-1} \sum_{j=n_0}^{n_0+n_p-1} [(1+\gamma)S_i^x S_j^x + (1-\gamma)S_i^y S_j^y] + \Delta K \sum_{i=0}^{n_0-1} \sum_{j=n_0}^{n_0+n_p-1} S_i^z S_j^z, \quad (1)$$

Here, i and j are the spin indices corresponding to the central and the peripheral spins respectively, $S_i^\alpha = \sigma_i^\alpha/2$ is the standard representation of spin operators corresponding to the lattice site i , with σ^α being the Pauli matrices, $\alpha = x, y, z$, and K is the strength of the exchange interaction. The dimensionless parameters γ and Δ respectively represent the xy - and the z -anisotropy corresponding to all pairs of spins, with $-1 \leq \gamma \leq 1$ and $-1 \leq \Delta \leq 1$. The Hamiltonian H_s represents a number of paradigmatic quantum spin Hamiltonians on the star network for different values of γ and Δ , including the XY model ($0 < |\gamma| < 1$, $\Delta = 0$), the XX model ($\gamma = 0$, $\Delta = 0$) the classical Ising model ($\gamma = \pm 1$, $\Delta = 0$), the isotropic Heisenberg model ($\gamma = 0$, $\Delta = 1$), and the Heisenberg model with a z -anisotropy ($\gamma = 0$, $0 < |\Delta| < 1$). In this paper, we consider the most general XYZ model ($0 < |\gamma| < 1$, $0 < |\Delta| < 1$) on the spin-star system in all three limits.

B. Entanglement in the star network of spins

To quantify entanglement in subsystems of the star network of spins in the state ρ , we consider two separate approaches, namely, (a) the partial trace-based approach, and (b) the measurement-based approach. The descriptions of these approaches are given below.

a. Partial trace-based approach. Let us consider a bipartition $A : B$ of the system, where we aim to quantify entanglement in B . The size of the individual partitions A and B are respectively determined by the number of spins N_A and N_B in them. In the partial trace-based approach, the state ρ_B on B is determined by tracing out the spin degrees of freedom corresponding to all spins $a = 1, 2, \dots, N_A$ in A , i.e.,

$$\rho_B = \text{Tr}_A[\rho]. \quad (2)$$

Using ρ_B , a suitable bipartite or a multipartite entanglement measure $E_B = E(\rho_B)$ is computed over the spins $b = 1, 2, \dots, N_B$ in B [1]. In this paper, we consider the situation where A is constituted only of the central spins, thereby having size $N_A = n_0$, while the peripheral spins constitute the partition B of size $N_B = n_p$. We specifically focus on bipartite entanglement measures on B , and denote

a bipartition of B as $B_1 : B_2$, with partitions B_1 and B_2 being of the sizes n' and $n_p - n'$ respectively. For even n_p , $1 \leq n' \leq n_p/2$, while for odd n_p , $1 \leq n' \leq (n_p - 1)/2$. Without any loss in generality, we assume that the spins $b = 1, 2, \dots, n' \in B_1$, and $b = n' + 1, n' + 2, \dots, n_p \in B_2$. For clarity, we denote $E_B \equiv E_{B_1:B_2}$.

b. Measurement-based approach. On the other hand, in the measurement based approach [32–35], independent projection measurements are performed on all spins in A , giving rise to an ensemble of post-measured states

$$\varrho_{\mathbf{k}} = \frac{1}{p_{\mathbf{k}}} [(P_A^{\mathbf{k}} \otimes I_B)\rho(P_A^{\mathbf{k}} \otimes I_B)], \quad (3)$$

where each state $\varrho_{\mathbf{k}}$ has a probability of occurrence $p_{\mathbf{k}} = \text{Tr}[(P_A^{\mathbf{k}} \otimes I_B)\rho(P_A^{\mathbf{k}} \otimes I_B)]$, with $P_A^{\mathbf{k}} = |\mathbf{k}\rangle\langle\mathbf{k}|$ being the projector corresponding to the measurement-basis $|\mathbf{k}\rangle$. For independent projection measurements on all spins in A ,

$$P_A^{\mathbf{k}} = \otimes_{a \in A} |\mathbf{k}_a\rangle\langle\mathbf{k}_a|, \quad (4)$$

with $\mathbf{k}_a = \mathbf{0}, \mathbf{1}$, where

$$|\mathbf{0}_a\rangle = \cos \frac{\theta_a}{2} |0_a\rangle + e^{i\phi_a} \sin \frac{\theta_a}{2} |1_a\rangle, \\ |\mathbf{1}_a\rangle = \sin \frac{\theta_a}{2} |0_a\rangle - e^{i\phi_a} \cos \frac{\theta_a}{2} |1_a\rangle, \quad (5)$$

$\{|0_a\rangle, |1_a\rangle\}$ being the computational basis. For each measurement outcome \mathbf{k} on A , the post-measured state $\varrho_{\mathbf{k}}$ has the form

$$\varrho_{\mathbf{k}} = P_A^{\mathbf{k}} \otimes \varrho_B^{\mathbf{k}}, \quad (6)$$

so that an average entanglement over the ensemble of all possible post-measured states on B can be defined as $\sum_{\mathbf{k}} p_{\mathbf{k}} E_B^{\mathbf{k}}$, with $E_B^{\mathbf{k}} = E(\varrho_B^{\mathbf{k}})$ is an entanglement measure, bipartite or multipartite, computed with the state $\varrho_B^{\mathbf{k}}$ on B . A maximization of $\langle E_B \rangle$ with respect to the $2N_A$ real parameters $\{\theta_a, \phi_a\} \forall a \in A$ leads to the definition of *localizable entanglement* [33–35] over the subsystem B , given by

$$\langle E_B \rangle = \max_{\{\theta_a, \phi_a\}} \left[\sum_{\mathbf{k}} p_{\mathbf{k}} E_B^{\mathbf{k}} \right], \quad (7)$$

via single-spin projection measurements over all spins in A . Similar to the case of the partial trace-based approach, we focus on bipartition $B_1 : B_2$ in B , and write $E_B^{\mathbf{k}} = E_{B_1:B_2}^{\mathbf{k}}$, and $\langle E_B \rangle = \langle E_{B_1:B_2} \rangle$. Note that the basis-independence of partial trace and the convexity property [1] of the chosen entanglement measure E implies

$$\langle E_{B_1:B_2} \rangle \geq E_{B_1:B_2}. \quad (8)$$

To quantify bipartite entanglement over a partition $B_1 : B_2$ in a state ρ_B (or $\varrho_B^{\mathbf{k}}$) on B , we use *logarithmic negativity* [37] as an entanglement measure, defined as

$$\mathcal{L} = \log_2(\mathcal{N} + 1), \quad (9)$$

where \mathcal{N} is the *negativity* [38] of ρ_B , defined as

$$\mathcal{N} = \|\rho_B^{T_{B_1}}\| - 1 = 2 \left| \sum_{\lambda_i < 0} \lambda_i \right|. \quad (10)$$

Here, $\rho_B^{T_{B_1}}$ is the partially transposed density matrix ρ_B with respect to the subsystem B_1 , $\|\cdot\|$ denotes the trace norm, and λ are the negative eigenvalues of $\rho_B^{T_{B_1}}$.

III. XYZ MODEL ON A STAR NETWORK IN THE LARGE PERIPHERY LIMIT

We now consider the XYZ model on a star network of spins in the large periphery limit. We choose the case of a single central spin ($n_0 = 1$), and increase n_p in order to attain this limit. We identify $|K|$ as the natural energy scale of the system, and write the dimensionless spin-star Hamiltonian $H_s/|K| \rightarrow H_s$ as

$$H_s = \pm \frac{1}{2} \{S_0^+(J_p^- + \gamma J_p^+) + S_0^-(J_p^+ + \gamma J_p^-)\} + \Delta S_0^z J_p^z, \quad (11)$$

where $J_p^\alpha = \sum_{i=1}^{n_p} S_i^\alpha$, $\alpha = x, y, z$, are defined on the Hilbert space of the peripheral spins, and the signs of H_s is determined by whether the spin-spin interaction is ferromagnetic (FM, $K > 0$) or antiferromagnetic (AFM, $K < 0$). Note that the operators J_p^α , $\alpha = x, y, z$, obeys the usual commutation and anticommutation relation of angular momentum operators, implying that the peripheral spins collectively behave as a spin- $n_p/2$ particle with the spin operator $\mathbf{J}_p = (J_p^x, J_p^y, J_p^z)$, while the total spin operator for the star network is given by $\mathbf{S}_0 + \mathbf{J}_p$, with $\mathbf{S}_0 = (S_0^x, S_0^y, S_0^z)$. We also define $S_i^\pm = S_i^x \pm iS_i^y$ for the i th spin, and subsequently $J_p^\pm = \sum_{i=1}^{n_p} S_i^\pm$.

A. Diagonalization

Since $[H_s, \mathbf{J}_p^2] = [H_s, \mathbf{S}_0^2] = 0$, H_s is block diagonal in the basis $|b\rangle = |S_0, m_0\rangle \otimes |J_p, m_p\rangle$, where

$$\begin{aligned} \mathbf{S}_0^2 |S_0, m_0\rangle &= S_0(S_0 + 1) |S_0, m_0\rangle, \\ \mathbf{J}_p^2 |J_p, m_p\rangle &= J_p(J_p + 1) |J_p, m_p\rangle. \end{aligned} \quad (12)$$

Noticing that

- (a) S_0 only has one allowed value $S_0 = \frac{1}{2}$ implying $m_0 = \pm 1/2$, and
- (b) different blocks of H_s corresponding to a fixed value of m_0 can be labelled by specific values of J_p , where m_p in each block can take $2J_p + 1$ values, $-J_p \leq m_p \leq J_p$,

for each block, it is sufficient to represent the basis as $|b\rangle = |m_0, m_p\rangle = |m_0\rangle \otimes |m_p\rangle$. Evidently, the ground state of H_s belongs to one of these blocks with a specific value of J_p . Our numerical analysis suggests that irrespective of the system size n , the ground state $|\Psi_0\rangle$ always belongs to the sector with $J_p = n_p/2$ (see, for example, [36] for a similar property in the LMG model), while the same is true for the first excited state $|\Psi_1\rangle$ for $n_p \geq 3$ (see Appendix A for a demonstration with $n_p = 2, 3$).

Let us now set $|m_i = \pm 1/2\rangle$ basis as the computational basis $\{|0\rangle \equiv |1/2\rangle, |1\rangle \equiv |-1/2\rangle\}$ for the spin i , such that

$$\begin{aligned} S_i^z |1/2\rangle &= (+1/2) |1/2\rangle, \\ S_i^z |-1/2\rangle &= (-1/2) |-1/2\rangle. \end{aligned} \quad (13)$$

Using this, we write the permutation-invariant Dicke state [34, 39] on the n_p peripheral spins with $n_p - l$ excitations:

$$|D_l^{n_p}\rangle = \frac{1}{\sqrt{\binom{n_p}{l}}} \sum_i \mathcal{P}_i \left(|1\rangle^{\otimes l} |0\rangle^{\otimes n_p-l} \right) \quad (14)$$

with the summation being over all possible permutations \mathcal{P}_i over n_p -spin product states, where l spins are in the ground state $|1\rangle$, and the rest $n_p - l$ spins are in the excited state $|0\rangle$, $0 \leq l \leq n_p$. Noting that

$$J_p^z |D_l^{n_p}\rangle = \lambda_l |D_l^{n_p}\rangle, \quad (15)$$

$$J_p^2 |D_l^{n_p}\rangle = \lambda |D_l^{n_p}\rangle, \quad (16)$$

$$J_p^\pm |D_l^{n_p}\rangle = \left[\lambda - \lambda_l (\lambda_l \pm 1) \right]^{\frac{1}{2}} |D_{l\mp 1}^{n_p}\rangle, \quad (17)$$

where $\lambda_l = \frac{n_p}{2} - l$ and $\lambda = \frac{n_p}{2} \left(\frac{n_p}{2} + 1 \right)$, we further identify

$$|D_l^{n_p}\rangle \equiv \left| J_p = \frac{n_p}{2}, m_p = \frac{n_p}{2} - l \right\rangle; \quad 0 \leq l \leq n_p. \quad (18)$$

Therefore, the $J_p = n_p/2$ block of H_s , which we denote by $\mathcal{H}_{n_p/2}$, is a $2(n_p + 1)$ -dimensional subspace spanned by the permutation-invariant n_p qubit Dicke states, with

$$|m_0, m_p\rangle \equiv |m_0\rangle \otimes |D_l^{n_p}\rangle; \quad 0 \leq l \leq n_p, \quad (19)$$

and $\mathcal{H}_{n_p/2}$ takes the form

$$\mathcal{H}_{n_p/2} = \begin{bmatrix} B & A \\ A^T & B' \end{bmatrix}, \quad (20)$$

with the matrix elements for the $n_p + 1$ dimensional matrices A and B as

$$\begin{aligned} A_{i,j} &= [\lambda - \lambda_j (\lambda_j - 1)]^{\frac{1}{2}} \delta_{i-1,j}/2 \\ &\quad + \gamma [\lambda - \lambda_j (\lambda_j + 1)]^{\frac{1}{2}} \delta_{i+1,j}/2, \end{aligned} \quad (21)$$

$$B_{i,j} = \Delta \lambda_i \delta_{i,j}/2 = -B'_{i,j}, \quad (22)$$

where $i, j \in [0, n_p]$. Due to the linear increase in dimension with increasing n_p , $\mathcal{H}_{n_p/2}$ can be numerically diagonalized to obtain the ground state of the model even for large n_p .

We further re-arrange the basis corresponding to the subspace hosting $\mathcal{H}_{n_p/2}$ such that $\mathcal{H}_{n_p/2}$ takes the form

$$\mathcal{H}_{n_p/2} = \begin{bmatrix} A_1 & 0 \\ 0 & A_2 \end{bmatrix}, \quad (23)$$

where each of A_1, A_2 are $(n_p + 1)$ -dimensional matrices, and the basis has been grouped as

$$\begin{aligned} A_1 &: \{|1/2\rangle |-n_p/2 + 2k\rangle, |-1/2\rangle |-n_p/2 + 2k + 1\rangle\}, \\ A_2 &: \{|-1/2\rangle |-n_p/2 + 2k + 1\rangle, |1/2\rangle |-n_p/2 + 2k\rangle\}, \end{aligned} \quad (24)$$

with $0 \leq k \leq n_p/2$ for even n_p , and $0 \leq k \leq (n_p - 1)/2$ when n_p is odd. The utility of this re-arrangement will be clear in subsequent discussions.

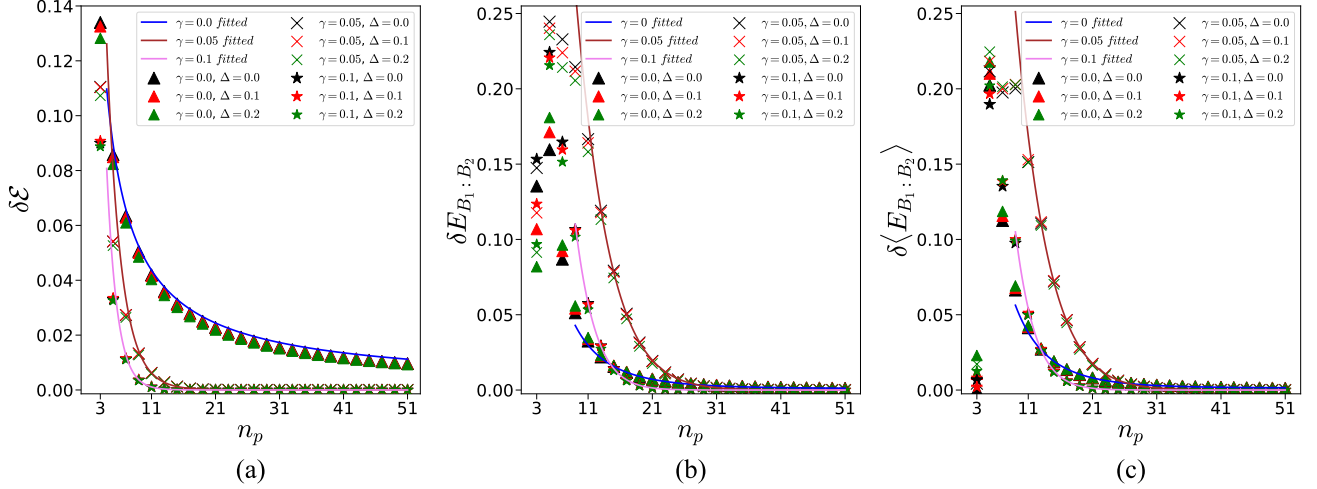


FIG. 2. Variations of (a) $\delta\mathcal{E}$, (b) $\delta E_{B_1:B_2}$, and (c) $\delta\langle E_{B_1:B_2} \rangle$ as functions of n_p for different values of γ and Δ , when n is even. The fitting parameters corresponding to $\delta\mathcal{E}$ (Eq. (27)) and $\delta E_{B_1:B_2}$ and $\delta\langle E_{B_1:B_2} \rangle$ (Eq. (31)) can be found in Table I (see Appendix B). All quantities plotted are dimensionless.

B. On ground state degeneracy

Let us now define

$$\mathcal{O} = S_0^x \bigotimes_{i=1}^{n_p} S_i^x, \quad (25)$$

where $[H_s, \mathcal{O}] = 0$. We first focus on the case of even n_p , and notice that \mathcal{O} connects the basis elements corresponding to A_1 and that corresponding to A_2 . Let us denote the eigenstate corresponding to the ground state energy \mathcal{E}_0 coming from A_1 is $|\psi_0\rangle_{A_1}$, and the same for A_2 is $|\psi_0\rangle_{A_2}$, while $|\psi_0\rangle_{A_1} = \mathcal{O} |\psi_0\rangle_{A_2}$, and vice-versa. The doubly-degenerate (DD) ground state of the system in the common eigenspace of \mathcal{O} and H_s is given by (see Appendix A for an example)

$$|\Psi_0^\pm\rangle = \frac{1}{\sqrt{2}} (|\psi_0\rangle_{A_1} \pm |\psi_0\rangle_{A_2}). \quad (26)$$

The double degeneracy in the ground state of H_s is found for all the allowed values of $0 \leq |\gamma| \leq 1$, and $0 \leq |\Delta| < 1$ when n_p is even (i.e., when $n = n_p + 1$ is odd).

On the other hand, in the case of odd n_p (i.e., for even $n = n_p + 1$), application of \mathcal{O} on the eigenstates of A_1 (A_2) does not take the state out of the subspace of A_1 (A_2). Apart from the lines $|\Delta| = 1$ in the (γ, Δ) parameter space where the ground state is DD (see Appendix A for examples), at all other allowed values of the anisotropy parameters ($0 \leq |\gamma| < 1$ ¹ and $0 \leq |\Delta| < 1$), the ground state is non-degenerate (ND). However, the energy gap $\delta\mathcal{E} = \mathcal{E}_1 - \mathcal{E}_0$ of the system, \mathcal{E}_1 (\mathcal{E}_0) being the energy corresponding to the first excited

(ground) state, decreases with increasing n_p as (see Fig. 2)

$$\delta\mathcal{E} \sim \begin{cases} a + bn_p^{-m} & \text{for } \gamma = 0 \\ a + \exp(-bn_p^m) & \text{for } \gamma \neq 0 \end{cases} \quad (27)$$

where the parameters a , b and m can be obtained by fitting numerical data, as shown in Table I (see Appendix B). For $\gamma = 0$, $\delta\mathcal{E}$ decreases slowly, and *vanishes*² when the periphery-size n_p is beyond a critical value $n_p^c \geq 5 \times 10^3$ (i.e., when the system size is beyond a critical size $n_c = 1 + n_p^c$). This critical periphery-size, n_p^c , is a function of the chosen system parameters (γ, Δ) . The collapse of $\delta\mathcal{E} \rightarrow 0$ becomes more rapid as the value of γ increases, and is achieved for $n_p^c \geq 13$, when $\gamma \geq 10^{-1}$, while the effect of Δ on n_p^c for a fixed γ is nominal (see Fig. 3). For $n_p \geq n_p^c$ with odd n_p , the ground states of the system, denoted by $|\Psi_0^\pm\rangle$ for consistency with energy eigenvalues \mathcal{E}_1 and \mathcal{E}_0 respectively, can be considered to be *effectively* DD (EDD).

Noticing the invariance of H_s under permutation of spins on the periphery irrespective of the value of n_p , the general form of the ground state $|\Psi_0\rangle$ (degenerate, or non-degenerate), obtained from diagonalizing $\mathcal{H}_{n_p/2}$, can be written as

$$|\Psi_0\rangle = \sum_{l=0}^{n_p} \frac{c_l}{\sqrt{2}} |\psi_0\rangle \otimes |D_l^{n_p}\rangle + \sum_{l'=0}^{n_p} \frac{d_{l'}}{\sqrt{2}} |\psi_0^\perp\rangle \otimes |D_{l'}^{n_p}\rangle, \quad (28)$$

where $\sum_{l=0}^{n_p} |c_l|^2 = \sum_{l'=0}^{n_p} |d_{l'}|^2 = 1$, and $\{|\psi_0\rangle, |\psi_0^\perp\rangle\}$ constitute a complete orthonormal basis in the Hilbert space of the central spin. The coefficients $\{c_l\}$ and $\{d_{l'}\}$ can be obtained by diagonalizing $\mathcal{H}_{n_p/2}$. If the ground state is doubly

¹ At $\gamma = 1$, ground states in the cases of both odd and even n_p are doubly degenerate.

² We assume $\delta\mathcal{E} = 0$ when $\delta\mathcal{E} < 10^{-4}$. This, indeed, depends on one's precision of numerical simulation.

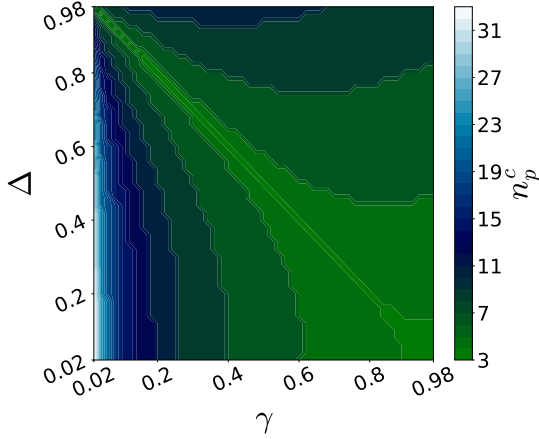


FIG. 3. Variation of n_p^c as a function of γ and Δ in the ranges $0 < \gamma, \Delta < 1$. All quantities plotted are dimensionless.

degenerate, one works with the *thermal ground state* (TGS) of H_s [40], given by an equal mixture of the degenerate ground states $|\Psi_0^\pm\rangle$ as

$$\rho_0 = \frac{1}{2} (|\Psi_0^+\rangle\langle\Psi_0^+| + |\Psi_0^-\rangle\langle\Psi_0^-|). \quad (29)$$

In the case of EDD ground states occurring for large odd n_p , one can also work with ρ_0 , and consider it as the *effective* TGS (ETGS), as there is negligible difference between \mathcal{E}_0 and \mathcal{E}_1 .

C. Static entanglement properties: Anisotropy effect

In this paper, we are interested in the partial trace-based and measurement-based quantification of entanglement in $|\Psi_0\rangle$ (for ND ground state), or ρ_0 (for DD or EDD ground state). We note that tracing out the central spin from either of these two states leads to a state of the form

$$\rho_p = \sum_{l,l'=0}^{n_p} c_{l,l'} |D_l^{n_p}\rangle\langle D_{l'}^{n_p}|, \quad (30)$$

for which prescription for computing entanglement $E_{B_1:B_2}$, quantified by the negativity or the logarithmic negativity, over arbitrary bipartition $B_1 : B_2$ exists [41]. On the other hand, a projection measurement on the central spin in the basis $\{|0\rangle, |1\rangle\}$ results in a post-measured ensemble $\{\rho_p^1, \rho_p^2\}$, with $\rho_p^{1,2}$ both being of the form (30), such that $\langle E_{B_1:B_2} \rangle$ can be computed. We point out here that the projection measurement on the central spin in the basis $\{|0\rangle, |1\rangle\}$ may not be optimal, and would only provide a lower bound corresponding to the actual localizable entanglement (see Eq. (7)). However, our numerical analysis for small systems indicate that for $n_0 \ll n_p$, $\{|0\rangle, |1\rangle\}$ is the optimal basis.

a. Peripheral entanglement of EDD states. Note that in the case of even n_p , the degenerate ground states $|\Psi_0^\pm\rangle$

are connected by the local unitary operator \mathcal{O} , and therefore have identical entanglement properties. However, this is not the case for odd n_p , and an interesting question would be how the two EDD states in the case of odd n_p differ from each other in terms of values of $E_{B_1:B_2}$ and $\langle E_{B_1:B_2} \rangle$ where n' is typically fixed at $n' = n_p/2$ for even n_p ($n' = (n_p - 1)/2$ for odd n_p), when n_p is increased. In Figs. 2(b), (c), we plot $\delta E_{B_1:B_2} = |E_{B_1:B_2}^+ - E_{B_1:B_2}^-|$ and $\delta \langle E_{B_1:B_2} \rangle = |\langle E_{B_1:B_2}^+ \rangle - \langle E_{B_1:B_2}^- \rangle|$ as functions of n_p for different values of γ and Δ , where the \pm in the superscripts in the expressions for $\delta E_{B_1:B_2}$ and $\delta \langle E_{B_1:B_2} \rangle$ denote the states $|\Psi_0^\pm\rangle$ (see discussions below Eq. (27)) for which entanglement is calculated. We find that $\delta E_{B_1:B_2}$ (and also $\delta \langle E_{B_1:B_2} \rangle$) approach zero as

$$\delta E_{B_1:B_2} \sim a + \exp(-bn_p^m), \quad (31)$$

similar to the $\gamma \neq 0$ case of Eq. (27) for the energy gap.

b. Peripheral entanglement against system-size. We now discuss the features of $E_{B_1:B_2}$ and $\langle E_{B_1:B_2} \rangle$ in the case of the XYZ model in the star network of spins with $n_0 = 1$. For demonstration, we choose $n' = n_p/2$ (for even n_p), and $(n_p - 1)/2$ (for odd n_p). Fig. 4(a)-(b) depicts the variations of $E_{B_1:B_2}$ and $\langle E_{B_1:B_2} \rangle$ as functions of n_p for different values of γ and Δ . The qualitative features of the partial trace-based and the measurement-based entanglement are similar, as indicated from Fig. 4. It is important to note that on the (γ, Δ) plane for odd n_p , the onset of $\delta \mathcal{E} = 0$ (i.e., n_p^c) is different for different points. This is indicated by the discontinuities in the variations of entanglement for odd n_p , computed from the ND ground state $|\Psi_0\rangle$ (Eq. (28)) for $n_p \leq n_p^c$, and from the mixed ETGS ρ_0 (Eq. (29)) for $n_p > n_p^c$. For $\gamma = 0$, $E_{B_1:B_2}$ (and also $\langle E_{B_1:B_2} \rangle$) exhibit a logarithmic dependence on n_p as

$$E_{B_1:B_2} \sim a + b \log_2 n_p, \quad (32)$$

where the fitting parameters a and b can be obtained by fitting the data for $E_{B_1:B_2}$ and $\langle E_{B_1:B_2} \rangle$ against n_p (see Fig. 4(a)-(b) for the example of $\Delta = 0$) when $n_p > n_p^c$. Also our numerical analysis suggest that for $\gamma = 0$, a and b depends on the choice of Δ weakly for even n_p , and are independent of Δ for odd n_p . However, in stark contrast, the logarithmic dependence is absent for $\gamma \neq 0$. This result indicate a prominent change in the variations of $E_{B_1:B_2}$ and $\langle E_{B_1:B_2} \rangle$ with periphery-size for vanishing and non-vanishing anisotropy parameter γ . We refer to this as the *anisotropy effect*. We point out here that this feature is unchanged for all constant ratios n'/n_p , where for the logarithmic dependence on n_p in case of $\gamma = 0$, only values of a and b change.

For a fixed periphery-size n_p (and subsequently for a fixed system-size n) and a varying partition size n' where the maximum value of n' is typically $n_p/2$, for all γ , $E_{B_1:B_2}$ (and $\langle E_{B_1:B_2} \rangle$) vary as

$$E_{B_1:B_2} \sim a [1 - \exp(-b(n')^m)], \quad (33)$$

which is demonstrated in Figs. 4(c)-(d) for both types of entanglement. Note that for $\gamma = 0$, the fitting parameters a, b and m remains unaffected up to three decimal places for

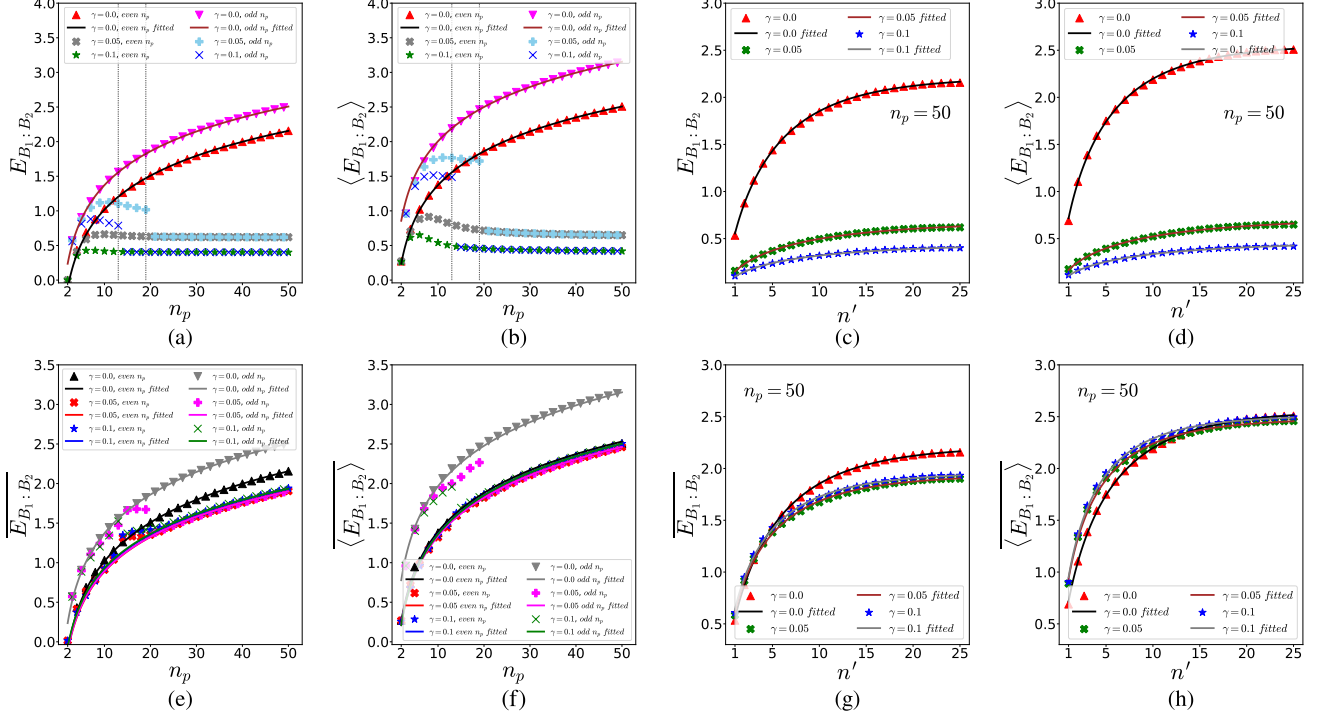


FIG. 4. Variations of (a) $E_{B_1:B_2}$, (b) $\langle E_{B_1:B_2} \rangle$, (e) $\overline{E_{B_1:B_2}}$ and (f) $\langle \overline{E_{B_1:B_2}} \rangle$ as functions of n_p for different values of γ , where $\Delta = 0$ and $n' = n_p/2$ ($(n_p - 1)/2$) when n_p is even (odd). The data for different γ are fitted to Eq. (32) for (a)-(b) $n_p \geq 20$ and (e)-(f) $n_p \geq 24$. In (a)-(b) the values of n_p^c are $n_p^c = 4999$ for $\gamma = 0$ (not shown in the figure), $n_p^c = 19$ for $\gamma = 0.05$, and $n_p^c = 13$ for $\gamma = 0.1$. We also plot the variations of (c) $E_{B_1:B_2}$, (d) $\langle E_{B_1:B_2} \rangle$, (g) $\overline{E_{B_1:B_2}}$ and (h) $\langle \overline{E_{B_1:B_2}} \rangle$ with n' where γ is varied and $\Delta = 0$, $n_p = 50$. The data are fitted to Eq. (33). The fitting parameters are provided in Table I (see Appendix B). All quantities plotted are dimensionless.

$\langle E_{B_1:B_2} \rangle$ when $0 \leq \Delta < 1$. For $E_{B_1:B_2}$, fitting parameter a has slight dependence on Δ which changes even the first decimal place. Whereas fitting parameters b and c remain unchanged up to two and three decimal places respectively. On the other hand, for $\gamma \neq 0$, all the fitting parameters depends on Δ .

D. Field-induced dynamics of entanglement

We now consider a situation where a time-dependent local magnetic field of strength $f(t)$ is applied to all spins in the star network. The field strength is such that

$$f(t) = \begin{cases} 0; & t = 0 \\ h; & t > 0 \end{cases}, \quad (34)$$

where $h > 0$ (see [42, 43] for use of similar magnetic field). The system at $t > 0$ therefore evolves in time due to the time-independent Hamiltonian

$$H_{\text{tot}} = H_s + h \sum_{i=0}^{n_0+n_p-1} S_i^z, \quad (35)$$

where we redefine $h \rightarrow h/|K|$ to keep H_{tot} dimensionless. Note that the features of block-diagonalization of H discussed in Sec. III A remain unchanged for H_{tot} also, irrespective of the value of h .

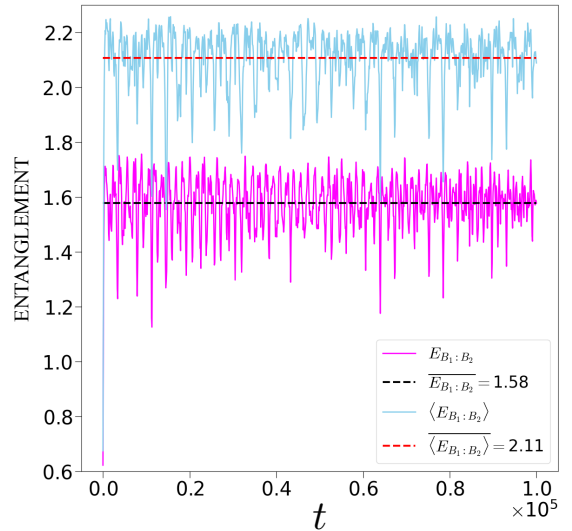


FIG. 5. A typical snapshot of the time-variations of $E_{B_1:B_2}$ and $\langle E_{B_1:B_2} \rangle$. The horizontal lines represent $\overline{E_{B_1:B_2}}$ and $\langle \overline{E_{B_1:B_2}} \rangle$. All quantities plotted are dimensionless.

Starting from an initial state ρ_0 of the system, the time-evolved state of the full system at time t is given by

$$\rho(t) = e^{-iH_{\text{tot}}t} \rho_0 e^{iH_{\text{tot}}t}. \quad (36)$$

The time-dependence of the partial trace-based entanglement on the peripheral qubits can be computed using $\rho_p(t) = \text{Tr}_0(\rho(t))$, while the measurement-based entanglement can be computed by performing single-qubit projective measurements on the central qubit, when the system is in state $\rho(t)$. In Fig. 5, we plot the time-evolution of $E_{B_1:B_2}$ and $\langle E_{B_1:B_2} \rangle$ for a system with $n_p = 30$, and $n' = 15$. Both $E_{B_1:B_2}$ and $\langle E_{B_1:B_2} \rangle$ oscillate with t , and the average values, $\overline{E_{B_1:B_2}}$ and $\langle \overline{E_{B_1:B_2}} \rangle$, are obtained by averaging over the time-series data in the long-time limit. We probe the long-time limit of the time-evolving spin-star system using $\overline{E_{B_1:B_2}}$ and $\langle \overline{E_{B_1:B_2}} \rangle$. Note that for $\gamma = 0$, the field term commutes with the Hamiltonian irrespective of Δ , leading to no time-evolution of the initial state. Therefore, we specifically focus on the cases with $\gamma \neq 0$. In Figs. 4(e) and (f), we respectively plot $\overline{E_{B_1:B_2}}$ and $\langle \overline{E_{B_1:B_2}} \rangle$ as functions of n_p , where the partition-size $n' = n_p/2$ ($(n_p - 1)/2$) for even (odd) n_p . In contrast to the static case discussed in Sec. III C, for large n_p , both $\overline{E_{B_1:B_2}}$ and $\langle \overline{E_{B_1:B_2}} \rangle$ exhibit logarithmic growth with n_p in both xy -isotropic ($\gamma = 0$) and xy -anisotropic ($\gamma \neq 0$) conditions, thereby negating the *anisotropy effect*. The discrepancies in the logarithmic variation due to the finite-size of the system vanishes within $n_p \sim 20$. We further test the variations of $\overline{E_{B_1:B_2}}$ and $\langle \overline{E_{B_1:B_2}} \rangle$ with n' for a fixed n_p , and found them to be similar to the static case (see Eq. (33)). See Figs. 4(g)-(h).

E. Large center limit

We now consider the XYZ model on the star network of spins when the size of the center is far larger than the size of the periphery, i.e., $n_0/n_p \gg 1$. Note that this limit is identical to the $n_0/n_p \ll 1$ limit of the model through an interchange of the central spins with peripheral spins, thereby exhibiting similar features of ground state energy as the limit $n_0/n_p \ll 1$. We present the variation of $E_{B_1:B_2}$ with n_0 for a fixed n_p in the limit $n_0/n_p \gg 1$ in Fig. 6(a) (the minimal instance of two peripheral spins and n_p central spins is represented in Fig. 1(b)). Our numerical analysis suggests that in contrast to the results obtained in the limit $n_0/n_p \ll 1$, for increasing n_0 with $n_0/n_p \gg 1$, $E_{B_1:B_2}$ decreases monotonically and approaches zero asymptotically as

$$E_{B_1:B_2} \sim a + bn_0^{-m}, \quad (37)$$

where the fitting parameters are obtained from the numerical data (see Fig. 6(a)).

IV. XYZ MODEL ON A STAR NETWORK IN THE COMPETING CENTER LIMIT

A question that naturally arises at this point is whether the features of bipartite peripheral entanglement remain the same as one considers the limit $n_0/n_p \rightarrow 1$. In this situation, the dimensionless spin-star Hamiltonian is given by

(see Eq. (11))

$$H_s = \pm \frac{1}{2} \left[J_0^+ (J_p^- + \gamma J_p^+) + J_0^- (J_p^+ + \gamma J_p^-) + \Delta J_0^z J_p^z \right], \quad (38)$$

where $J_0^\pm = \sum_{i=0}^{n_0-1} S_i^\pm$, $J_0^z = \sum_{i=0}^{n_0-1} S_i^z$, $J_p^\pm = \sum_{i=n_0}^{n_0+n_p-1} S_i^\pm$, and $J_p^z = \sum_{i=n_0}^{n_0+n_p-1} S_i^z$. Analysis for the Hamiltonian (38) is similar to that of the Hamiltonian (11) in the case of the single central spin, and the values of J_0 and J_p corresponding to the ground and the first excited states of H_s are $n_0/2$ and $n_p/2$ respectively, independent of the system parameters γ , and Δ . Upon diagonalization, doubly degenerate ground states are found when $n = n_0 + n_p$ is odd irrespective of the values of (γ, Δ) , while the effective degeneracy in ground states for large system size is observed when n is even only for $\gamma \neq 0$ (see Fig. 6(b)). Note that in the present case, $\delta\mathcal{E}$ approaches saturation (for $\gamma = 0$) or vanishing (for $\gamma \neq 0$) as

$$\delta\mathcal{E} \sim a + \exp(-bn_p^m). \quad (39)$$

For $\gamma = 0$, according to our numerical investigation up to $n_p = n_0 = 50$, $\delta\mathcal{E}$ saturates to a non-zero value, which increases with an increase in the value of Δ , implying a ND ground state for $\gamma = 0$ up to the maximum system-size investigated in this paper.

In the limit $n_0/n_p \rightarrow 1$, the structure of the ground states with permutation symmetry in both central and peripheral qubits is given by

$$|\Psi_0\rangle = \sum_{l'=0}^{n_0} \sum_{l=0}^{n_p} c_{l,l'} |D_{l'}^{n_0}\rangle \otimes |D_l^{n_p}\rangle, \quad (40)$$

where $\sum_{l'} \sum_l |c_{l,l'}|^2 = 1$, and the definition of $|D_{l'}^{n_0}\rangle$ is similar to that of $|D_l^{n_p}\rangle$. Similar to the case of single central qubit, the TGS ρ_0 corresponding to the degenerate and the effectively degenerate ground states $|\Psi_0^\pm\rangle$ is of the form (29), while the mixed state ρ_p on the peripheral qubits obtained via tracing out the central qubits is of the form (30), enabling one to compute the bipartite entanglement $E_{B_1:B_2}$ on the peripheral spins. In Fig. 6(c), we plot the variations of $E_{B_1:B_2}$ as a function of n_p , where $n_p = n_0$. In contrast to the limit $n_0/n_p \ll 1$, $E_{B_1:B_2}$ for $\gamma = 0$ saturates with increasing n_p as

$$E_{B_1:B_2} \sim a [1 - \exp(-bn_p^m)]. \quad (41)$$

For $\gamma \neq 0$ also, $E_{B_1:B_2}$ saturates with n_p , although the approach to saturation is different from that of the $\gamma = 0$, and the saturation value decreases with increasing γ , implying an *anisotropy effect*. However, the time-averaged bipartite peripheral entanglement, $\overline{E_{B_1:B_2}}$, in contrast to the $n_0/n_p \ll 1$ limit, does not negate the anisotropy effect.

V. CONCLUSION AND OUTLOOK

In this paper, we study the XYZ model on a spin-star system, where a number of central spins are connected to a

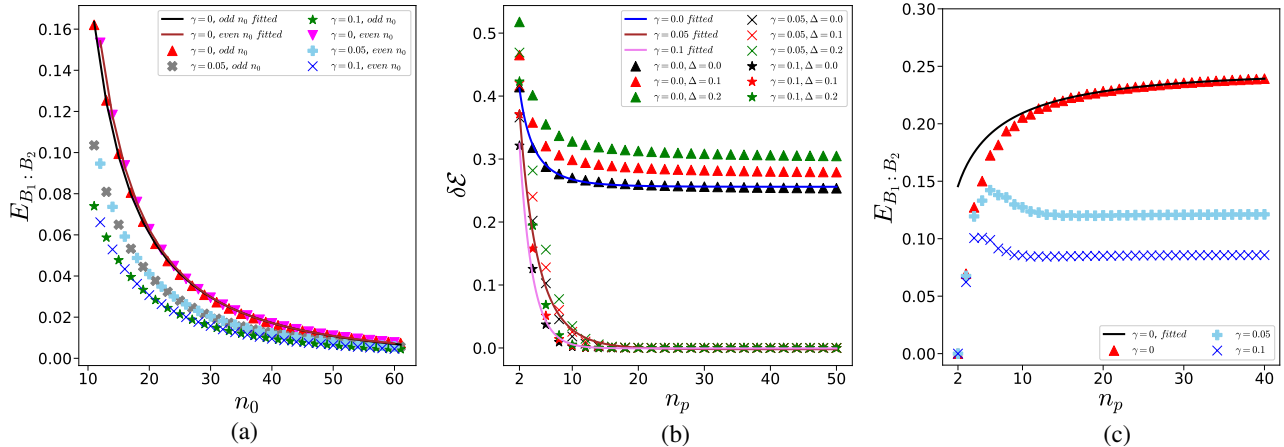


FIG. 6. (a) Variation of $E_{B_1:B_2}$ with n_0 in the limit $n_0/n_p \gg 1$, where n_p is fixed at $n_p = 10$. For $\gamma = 0$, the data is fitted to Eq. (37). (b)-(c) Variations of (b) $\delta\mathcal{E}$ and (c) $E_{B_1:B_2}$ with n_p in the limit $n_0/n_p \rightarrow 1$, where we fix $n_0 = n_p$. The data corresponding to $\Delta = 0$ in (b) are fitted to Eq. (39), while the same corresponding to $\gamma = 0$ in (c) are fitted to Eq. (41). See Table I (Appendix B) for the numerical values of the respective fitting parameters. All quantities plotted are dimensionless.

number of peripheral spins in such a way that each central spin interacts with all peripheral spins. We specifically consider the limit of the system where the number of central spins are very small compared to the number of peripheral spins. In this limit, the ground state of the system is doubly degenerate when the system-size is even, while there is a finite energy gap between the ground and the first excited states of the system with odd number of spins. This energy gap decreases rapidly with increasing system-size, inducing an *effective* double degeneracy of the ground states. When the system size is large (i.e., when the periphery-size is large), the bipartite entanglement over typically equal bipartition of the periphery, computed from either partial trace-based, or measurement-based approaches, exhibits a logarithmic growth with the periphery-size when the system is *xy*-isotropic (i.e., $\gamma = 0$). This feature vanishes for $\gamma \neq 0$, which we refer to as the anisotropy effect. Interestingly, the anisotropy effect can be nullified by kick-starting a magnetic field of constant strength on all spins in the system, where the average values of the time-series of bipartite peripheral entanglement computed from either of the approaches exhibit a logarithmic growth with the periphery-size irrespective of the values of γ . We further consider the large center and the competing center limits of the model, and find the features of bipartite peripheral entanglement to be qualitatively different from that of the large periphery limit of the model.

A number of possible research directions open up from this study. Within the range of the results reported in this paper, it would be interesting to investigate whether similar features in entanglement exists if interactions are present within the central and/or the peripheral spins themselves. Also, a similar investigation in a star-chain configuration of spin- $\frac{1}{2}$ particles [19] is yet to be performed. Another interesting question would be whether these entanglement properties of the spin-star system are robust against the presence of quenched disorder in the system [44]. Besides, similarity of our results with the already existing results for the LMG

model [36] raises the question as to what would be the underlying principle to model a spin-lattice system that exhibits similar entanglement properties. Moreover, recent interests in exploring quantum technological aspects involving *d*-level systems, or qudits [45] highlights the relevance of exploring similar models where lattice sites are populated with spins having a higher spin quantum number.

ACKNOWLEDGMENTS

We acknowledge the use of **QIClib** – a modern C++ library for general purpose quantum information processing and quantum computing. We also thank Aditi Sen (De) for useful discussions.

Appendix A: Small systems with single central spin

In this section, we look into two specific examples for $n_p = 2$ and $n_p = 3$ in the case of a star network of $(n_p + 1)$ spins, as follows.

1. $n_p = 2$

We first consider the case of $J_p = 1$ ($m_p = -1, 0, 1$) among the allowed values $J_p = 0, 1$ for $n_p = 2$. We group the basis states according to Eq. (24) as

$$\{|-1/2\rangle |-1\rangle, |1/2\rangle |0\rangle, |-1/2\rangle |1\rangle\}$$

and

$$\{|1/2\rangle |-1\rangle, |-1/2\rangle |0\rangle, |1/2\rangle |1\rangle\}$$

respectively, leading to the \mathcal{H}_1 block having the form (23), with A_1 and A_2 being two 3×3 matrices given by

$$A_1 = \frac{1}{2} \begin{bmatrix} -\Delta & 0 & \alpha_0^- \\ 0 & \Delta & \gamma\alpha_0^+ \\ \alpha_{-1}^+ & \gamma\alpha_1^- & 0 \end{bmatrix}, \quad (\text{A1})$$

$$A_2 = \frac{1}{2} \begin{bmatrix} 0 & \gamma\alpha_{-1}^+ & \alpha_1^- \\ \gamma\alpha_0^- & \Delta & 0 \\ \alpha_0^+ & 0 & -\Delta \end{bmatrix}, \quad (\text{A2})$$

upto a normalization factor, where

$$\alpha_{m_p}^\pm = \sqrt{J_p(J_p + 1) - m_p(m_p \pm 1)}. \quad (\text{A3})$$

Note that $|A_1| = |A_2| = 2\Delta(\gamma^2 - 1)$, which vanishes for $\Delta = 0$ or $\gamma = \pm 1$, implying that at least one of the eigenvalues of both A_1 and A_2 vanishes at these conditions. For $\Delta = 0$, the eigenvalues are $0, \pm\sqrt{2(\gamma^2 + 1)}/2$ for both A_1 and A_2 , leading to the doubly-degenerate ground state energy $-\sqrt{2(\gamma^2 + 1)}/2$. The corresponding eigenvectors belonging to the blocks A_1 and A_2 are given by

$$\begin{aligned} |\psi\rangle_{0,A_1} &= \frac{1}{\sqrt{2(\gamma^2 + 1)}} |-1/2\rangle_0 \left(|-1\rangle_p + \gamma |1\rangle_p \right) \\ &\quad - \frac{1}{\sqrt{2}} |1/2\rangle_0 |0\rangle_p, \\ |\psi\rangle_{0,A_2} &= \frac{1}{\sqrt{2(\gamma^2 + 1)}} |1/2\rangle_0 \left(\gamma |-1\rangle_p + |1\rangle_p \right) \\ &\quad - \frac{1}{\sqrt{2}} |-1/2\rangle_0 |0\rangle_p, \end{aligned} \quad (\text{A4})$$

where clearly $|\psi\rangle_{0,A_1} = \mathcal{O} |\psi\rangle_{0,A_2}$, and vice-versa (see Sec. III B). Consequently, the doubly degenerate ground-states corresponding to the ground-state energy $-\sqrt{2(\gamma^2 + 1)}/2$ and in the common eigenspace of H_s and \mathcal{O} are given by Eq. (26). Similarly for $\gamma = \pm 1$, the eigenvalues of either of A_1 and A_2 are $0, \pm\sqrt{4 + \Delta^2}/2$, with the doubly-degenerate ground state energy $-\sqrt{4 + \Delta^2}/2$, and the corresponding eigenvectors being

$$\begin{aligned} |\psi\rangle_{0,A_1} &= \left(\frac{\sqrt{4 + \Delta^2} - \Delta}{\sqrt{4 + \Delta^2} + \Delta} \right) |-1/2\rangle_0 |1\rangle_p \\ &\quad + |-1/2\rangle_0 |-1\rangle_p + \left(\frac{\Delta - \sqrt{4 + \Delta^2}}{\sqrt{2}} \right) |1/2\rangle_0 |0\rangle_p, \\ |\psi\rangle_{0,A_2} &= \left(\frac{\sqrt{4 + \Delta^2} - \Delta}{\sqrt{4 + \Delta^2} + \Delta} \right) |1/2\rangle_0 |-1\rangle_p \\ &\quad + |1/2\rangle_0 |1\rangle_p + \left(\frac{\Delta - \sqrt{4 + \Delta^2}}{\sqrt{2}} \right) |-1/2\rangle_0 |0\rangle_p, \end{aligned} \quad (\text{A5})$$

upto a normalization factor. It is easy to see that similar to the case of $\Delta = 0$, $|\psi\rangle_{0,A_1}$ and $|\psi\rangle_{0,A_2}$ are connected via \mathcal{O} , and the doubly-degenerate ground states in the common eigenspace of H_s and \mathcal{O} are given by Eq. (26), as in the case of $\Delta = 0$. The double degeneracy in ground state is maintained in the entire range $0 \leq |\gamma| \leq 1, 0 \leq |\Delta| \leq 1$.

We point out here that all sectors of H_s corresponding to values of $J_p \neq n_p/2$ can be block-diagonalized using a similar grouping of basis elements. In the present example, the

block \mathcal{H}_0 corresponding to $J_p = 0$, is diagonal in the basis $\{|\frac{1}{2}\rangle \otimes |0\rangle, |-\frac{1}{2}\rangle \otimes |0\rangle\}$, with both eigenvalues vanishing irrespective of the values of (γ, Δ) .

2. $n_p = 3$

In this case, $J_p = 3/2, 1/2, 1/2$, and we start with the block $H_s(J_p = 3/2)$, where grouping the basis as

$$\{|-1/2\rangle |3/2\rangle, |1/2\rangle |1/2\rangle, |-1/2\rangle |-1/2\rangle, |1/2\rangle |-3/2\rangle\}$$

and

$$\{|1/2\rangle |3/2\rangle, |-1/2\rangle |1/2\rangle, |1/2\rangle |-1/2\rangle, |-1/2\rangle |-3/2\rangle\}$$

makes $\mathcal{H}_{3/2}$ of the form (23) with the 4×4 matrices A_1 and A_2 given by

$$A_1 = \frac{1}{2} \begin{bmatrix} \frac{3\Delta}{2} & 0 & \gamma\alpha_{\frac{1}{2}}^+ & 0 \\ 0 & -\frac{\Delta}{2} & \alpha_{\frac{1}{2}}^+ & \gamma\alpha_{-\frac{3}{2}}^+ \\ \gamma\alpha_{\frac{3}{2}}^- & \alpha_{-\frac{1}{2}}^- & -\frac{\Delta}{2} & 0 \\ 0 & \gamma\alpha_{-\frac{1}{2}}^- & 0 & \frac{3\Delta}{2} \end{bmatrix}, \quad (\text{A6})$$

$$A_2 = \frac{1}{2} \begin{bmatrix} \frac{\Delta}{2} & 0 & \alpha_{\frac{3}{2}}^- & \gamma\alpha_{-\frac{1}{2}}^+ \\ 0 & -\frac{3\Delta}{2} & 0 & \alpha_{-\frac{1}{2}}^- \\ \alpha_{\frac{1}{2}}^+ & 0 & -\frac{3\Delta}{2} & 0 \\ \gamma\alpha_{\frac{1}{2}}^- & \alpha_{-\frac{3}{2}}^+ & 0 & \frac{\Delta}{2} \end{bmatrix} \quad (\text{A7})$$

The eigenvalues of $\mathcal{H}_{3/2}$ are

$$\begin{aligned} \lambda_{\pm}^1 &= \frac{1}{2} \left(\frac{\Delta}{2} + 1 \pm \sqrt{(\Delta - 1)^2 + 3\gamma^2} \right), \\ \lambda_{\pm}^2 &= \frac{1}{2} \left(\frac{\Delta}{2} - 1 \pm \sqrt{(\Delta + 1)^2 + 3\gamma^2} \right), \\ \lambda_{\pm}^3 &= \frac{1}{2} \left(-\frac{\Delta}{2} + \gamma \pm \sqrt{(\Delta + \gamma)^2 + 3} \right), \\ \lambda_{\pm}^4 &= \frac{1}{2} \left(-\frac{\Delta}{2} - \gamma \pm \sqrt{(\Delta - \gamma)^2 + 3} \right), \end{aligned} \quad (\text{A8})$$

none of which are degenerate for $\Delta = 0$ or $\gamma = 0$. On the other hand, $\mathcal{H}_{1/2}$ also takes the form (23) upon grouping the basis as

$$\{|1/2\rangle |1/2\rangle, |-1/2\rangle |-1/2\rangle\}$$

and

$$\{|1/2\rangle |-1/2\rangle, |-1/2\rangle |1/2\rangle\}$$

with the two-dimensional A_1 and A_2 matrices given as

$$A_1 = \frac{1}{2} \begin{bmatrix} \frac{\Delta}{2} & \gamma\alpha_{-\frac{1}{2}}^+ \\ \gamma\alpha_{\frac{1}{2}}^- & \frac{\Delta}{2} \end{bmatrix}, A_2 = \frac{1}{2} \begin{bmatrix} -\frac{\Delta}{2} & \alpha_{\frac{1}{2}}^- \\ \alpha_{-\frac{1}{2}}^+ & -\frac{\Delta}{2} \end{bmatrix}. \quad (\text{A9})$$

The eigenvalues of $\mathcal{H}_{1/2}$ are

$$\lambda_{\pm}^5 = \frac{\Delta}{4} \pm \frac{\gamma}{2}, \lambda_{\pm}^6 = -\frac{\Delta}{4} \pm \frac{1}{2}, \quad (\text{A10})$$

each of which is doubly degenerate due to the presence of a second identical block $\mathcal{H}_{1/2}$.

Note that for $\Delta = 0$ and for arbitrary *positive* values of γ within its allowed range, the ground state energy is given by either λ_-^4 , or λ_-^2 , depending on the value of γ . The eigenvectors corresponding to these two eigenvalues are given by

$$\begin{aligned} |\psi(\lambda_-^2)\rangle &= -|1/2\rangle|3/2\rangle - \frac{1 + \sqrt{1 + \gamma^2}}{\sqrt{3}\gamma} |1/2\rangle|1/2\rangle \\ &\quad + \frac{1 + \sqrt{1 + \gamma^2}}{\sqrt{3}\gamma} |-1/2\rangle|-1/2\rangle + |1/2\rangle|-3/2\rangle, \\ |\psi(\lambda_-^4)\rangle &= -|1/2\rangle|3/2\rangle + \frac{\gamma - \sqrt{3 + \gamma^2}}{\sqrt{3}} |-1/2\rangle|1/2\rangle \\ &\quad - \frac{\gamma - \sqrt{3 + \gamma^2}}{\sqrt{3}} |1/2\rangle|-1/2\rangle + |-1/2\rangle|-3/2\rangle, \end{aligned} \quad (\text{A11})$$

upto normalization, both of which are eigenvectors of \mathcal{O} with an eigenvalue -1 . Similar result can be obtained for negative values of γ as well. On the other hand, for $\gamma = 0$ and $0 < |\Delta| < 1$, the ground state is non-degenerate with the ground state eigenvalue given by λ_-^2 , and the corresponding eigenvector is

$$|\psi(\lambda_-^2)\rangle = \frac{1}{\sqrt{2}} (|-1/2\rangle|-1/2\rangle - |1/2\rangle|1/2\rangle). \quad (\text{A12})$$

For $\gamma = 0$ and $\Delta = 1$, the ground state is two-fold degenerate with eigenvalue $\lambda_-^3 (= \lambda_-^4)$ and corresponding eigenvectors,

upto normalization, are

$$\begin{aligned} |\psi(\lambda_-^3)\rangle &= \frac{a}{\sqrt{2}} (|1/2\rangle|3/2\rangle - |-1/2\rangle|-3/2\rangle) \\ &\quad + \frac{\sqrt{1 - a^2}}{\sqrt{2}} (|-1/2\rangle|1/2\rangle - |1/2\rangle|-1/2\rangle), \\ |\psi(\lambda_-^4)\rangle &= \frac{a}{\sqrt{2}} (|1/2\rangle|3/2\rangle + |-1/2\rangle|-3/2\rangle) \\ &\quad + \frac{\sqrt{1 - a^2}}{\sqrt{2}} (|-1/2\rangle|1/2\rangle + |1/2\rangle|-1/2\rangle), \end{aligned} \quad (\text{A13})$$

where

$$a = \frac{-(\Delta + \sqrt{3 + \Delta^2})}{\sqrt{3 + (\Delta + \sqrt{3 + \Delta^2})^2}} + \frac{\sqrt{3}}{\sqrt{3 + (\Delta - \sqrt{3 + \Delta^2})^2}}, \quad (\text{A14})$$

and we note that $\mathcal{O}|\psi(\lambda_-^2)\rangle = -|\psi(\lambda_-^2)\rangle$, $\mathcal{O}|\psi(\lambda_-^3)\rangle = -|\psi(\lambda_-^3)\rangle$, and $\mathcal{O}|\psi(\lambda_-^4)\rangle = |\psi(\lambda_-^4)\rangle$.

Appendix B: Fitting parameters

Here we present the information regarding the fitting of Eqs. (27), (31), (33), (37), (39), and (41) to the corresponding data presented in Figs. 2, 4, and 6. The fitting parameters a , b , and m in the above equations are consolidated in Table I.

-
- [1] R. Horodecki, P. Horodecki, M. Horodecki, and K. Horodecki, *Rev. Mod. Phys.* **81**, 865 (2009); O. Guhne and G. Toth, *Phys. Rep.* **474**, 1 (2009).
- [2] C. H. Bennett and S. J. Wiesner, *Phys. Rev. Lett.* **69**, 2881 (1992); C. H. Bennett, G. Brassard, C. Crepeau, R. Jozsa, A. Peres, and W. K. Wootters, *Phys. Rev. Lett.* **70**, 1895 (1993); K. Mattle, H. Weinfurter, P. G. Kwiat, and A. Zeilinger, *Phys. Rev. Lett.* **76**, 4656 (1996); D. Bouwmeester, J.-W. Pan, K. Mattle, M. Eibl, H. Weinfurter, and A. Zeilinger, *Nature* **390**, 575 (1997).
- [3] A. K. Ekert, *Phys. Rev. Lett.* **67**, 661 (1991); T. Jennewein, C. Simon, G. Weihs, H. Weinfurter, and A. Zeilinger, *Phys. Rev. Lett.* **84**, 4729 (2000); J. Yin, Y.-H. Li, S.-K. Liao, M. Yang, Y. Cao, L. Zhang, J.-G. Ren, W.-Q. Cai, W.-Y. Liu, S.-L. Li, R. Shu, Y.-M. Huang, L. Deng, L. Li, Q. Zhang, N.-L. Liu, Y.-A. Chen, C.-Y. Lu, X.-B. Wang, F. Xu, J.-Y. Wang, C.-Z. Peng, A. K. Ekert, and J.-W. Pan, *Nature* **582**, 501 (2020); C. Schimpf, M. Reindl, D. Huber, B. Lehner, S. F. C. D. Silva, S. Manna, M. Vyvlecka, P. Walther, and A. Rastelli, *Science Advances* **7**, eabe8905 (2021).
- [4] M. Dalmonte, B. Vermersch, and P. Zoller, *Nature Physics* **14**, 827 (2018); C. Kokail, R. van Bijnen, A. Elben, B. Vermersch, and P. Zoller, *Nature Physics* **17**, 936 (2021).
- [5] M. F. Riedel, P. Bohi, Y. Li, T. W. Hansch, A. Sinatra, and P. Treutlein, *Nature* **464**, 1170 (2010); J. Joo, W. J. Munro, and T. P. Spiller, *Phys. Rev. Lett.* **107**, 083601 (2011); R. Demkowicz-Dobrzanski and L. Maccone, *Phys. Rev. Lett.* **113**, 250801 (2014).
- [6] R. Raussendorf and H. J. Briegel, *Phys. Rev. Lett.* **86**, 5188 (2001); H. J. Briegel, D. E. Browne, W. Dur, R. Raussendorf, and M. Van den Nest, *Nat. Phys.* **5**, 19 (2009).
- [7] D. Bruß and C. Macchiavello, *Phys. Rev. A* **83**, 052313 (2011).
- [8] L. Amico, R. Fazio, A. Osterloh, and V. Vedral, *Rev. Mod. Phys.* **80**, 517 (2008); J. I. Latorre and A. Riera, *J. Phys. A: Math. Theor.* **42**, 504002 (2009); G. D. Chiara and A. Sanpera, *Reports on Progress in Physics* **81**, 074002 (2018).
- [9] D. Leibfried, R. Blatt, C. Monroe, and D. Wineland, *Rev. Mod. Phys.* **75**, 281 (2003); D. Porras and J. I. Cirac, *Phys. Rev. Lett.* **92**, 207901 (2004); X.-L. Deng, D. Porras, and J. I. Cirac, *Phys. Rev. A* **72**, 063407 (2005).
- [10] L. M. K. Vandersypen and I. L. Chuang, *Rev. Mod. Phys.* **76**, 1037 (2005); K. R. K. Rao, H. Katiyar, T. S. Mahesh, A. Sen (De), U. Sen, and A. Kumar, *Phys. Rev. A* **88**, 022312 (2013).
- [11] L.-M. Duan, E. Demler, and M. D. Lukin, *Phys. Rev. Lett.* **91**, 090402 (2003); O. Mandel, M. Greiner, A. Widera, T. Rom, T. W. Hansch, and I. Bloch, *Nature* **425**, 937 (2003); I. Bloch, *J. Phys. B: At. Mol. Opt. Phys.* **38**, S629 (2005); P. Treutlein, T. Steinmetz, Y. Colombe, B. Lev, P. Hommelhoff, J. Reichel, M. Greiner, O. Mandel, A. Widera, T. Rom, I. Bloch, and T. Hansch, *Fortschritte der Physik* **54**, 702 (2006); J. Simon, W. S. Bakr, R. Ma, M. E. Tai, P. M. Preiss, and M. Greiner, *Nature* **472**, 307 (2011); M. Cramer, A. Bernard, N. Fabbri,

Fig. No.	n odd/even	γ	a	b	m	Fig. No.	n odd/even	γ	a	b	m
Fig. 2(a)	even	0.0	0.0008	0.391	0.922	Fig. 4(e)	odd	0.0	-0.609	0.490	-
Fig. 2(a)	even	0.05	0.0	0.605	0.888	Fig. 4(e)	odd	0.05	-0.564	0.437	-
Fig. 2(a)	even	0.1	0.0	0.644	0.983	Fig. 4(e)	odd	0.1	-0.531	0.436	-
Fig. 2(b)	even	0.0	0.001	0.929	0.559	Fig. 4(f)	even	0.0	0.362	0.495	-
Fig. 2(b)	even	0.05	0.0	0.080	1.280	Fig. 4(f)	even	0.05	-0.276	0.485	-
Fig. 2(b)	even	0.1	0.0	0.131	1.285	Fig. 4(f)	even	0.1	-0.283	0.494	-
Fig. 2(c)	even	0.0	0.0014	0.705	0.644	Fig. 4(f)	odd	0.0	-0.253	0.489	-
Fig. 2(c)	even	0.05	0.0	0.086	1.265	Fig. 4(f)	odd	0.05	-0.249	0.480	-
Fig. 2(c)	even	0.1	0.0	0.133	1.288	Fig. 4(f)	odd	0.1	-0.283	0.494	-
Fig. 4(a)	even	0.0	-0.253	0.489	-	Fig. 4(g)	odd	0.0	2.218	0.287	0.798
Fig. 4(a)	odd	0.0	-0.609	0.490	-	Fig. 4(g)	odd	0.05	1.943	0.382	0.722
Fig. 4(b)	even	0.0	0.362	0.495	-	Fig. 4(g)	odd	0.1	1.966	0.394	0.727
Fig. 4(b)	odd	0.0	-0.253	0.489	-	Fig. 4(h)	odd	0.0	2.565	0.327	0.773
Fig. 4(c)	odd	0.0	2.218	0.287	0.798	Fig. 4(h)	odd	0.05	2.488	0.471	0.689
Fig. 4(c)	odd	0.05	0.688	0.247	0.714	Fig. 4(h)	odd	0.1	2.517	0.473	0.704
Fig. 4(c)	odd	0.1	0.449	0.245	0.706	Fig. 6(a)	odd	0.0	-0.004	7.624	1.591
Fig. 4(d)	odd	0.0	2.565	0.327	0.773	Fig. 6(a)	even	0.0	-0.002	1.123	1.719
Fig. 4(d)	odd	0.05	0.725	0.261	0.690	Fig. 6(b)	even	0.0	0.255	1.274	0.542
Fig. 4(d)	odd	0.1	0.471	0.258	0.682	Fig. 6(b)	even	0.05	-0.001	0.562	0.790
Fig. 4(e)	even	0.0	-0.253	0.489	-	Fig. 6(b)	even	0.1	-0.0006	0.588	0.934
Fig. 4(e)	even	0.05	-0.547	0.434	-	Fig. 6(c)	even	0.0	0.245	0.650	0.469
Fig. 4(e)	even	0.1	-0.505	0.432	-						

TABLE I. Values of fitting parameters a , b , and m from Eqs. (27), (31), (33), (37), (39), and (41), fitted to the corresponding data presented in Figs. 2, 4, and 6.

- L. Fallani, C. Fort, S. Rosi, F. Caruso, M. Inguscio, and M. B. Plenio, *Nature Communications* **4**, 2161 (2013).
- [12] M. Schechter and P. C. E. Stamp, *Phys. Rev. B* **78**, 054438 (2008).
- [13] S. Bose, *Phys. Rev. Lett.* **91**, 207901 (2003); S. Bose, A. Bayat, P. Sodano, L. Banchi, and P. Verrucchi, "Spin chains as data buses, logic buses and entanglers," in *Quantum State Transfer and Network Engineering*, edited by G. M. Nikolopoulos and I. Jex (Springer Berlin, Heidelberg, 2013) Chap. 1, pp. 1–38.
- [14] M. Hein, W. Dür, J. Eisert, R. Raussendorf, M. Van den Nest, and H. J. Briegel, *arXiv:quant-ph/0602096* (2006).
- [15] U. Schollwöck, *Rev. Mod. Phys.* **77**, 259 (2005); F. Verstraete, V. Murg, and J. Cirac, *Advances in Physics* **57**, 143 (2008); U. Schollwöck, *Annals of Physics* **326**, 96 (2011), january 2011 Special Issue; R. Orús, *Annals of Physics* **349**, 117 (2014); J. C. Bridgeman and C. T. Chubb, *Journal of Physics A: Mathematical and Theoretical* **50**, 223001 (2017).
- [16] F. Verstraete and J. I. Cirac, *arXiv:cond-mat/0407066* (2004); G. Vidal, *Phys. Rev. Lett.* **99**, 220405 (2007); *Phys. Rev. Lett.* **101**, 110501 (2008); M. Rizzi, S. Montangero, and G. Vidal, *Phys. Rev. A* **77**, 052328 (2008); M. Aguado and G. Vidal, *Phys. Rev. Lett.* **100**, 070404 (2008); L. Cincio, J. Dziarmaga, and M. M. Rams, *Phys. Rev. Lett.* **100**, 240603 (2008); G. Evenbly and G. Vidal, *Phys. Rev. B* **79**, 144108 (2009).
- [17] B. E. Kane, *Nature* **393**, 133 (1998); Y. Makhlin, G. Schön, and A. Shnirman, *Nature* **398**, 305 (1999); A. Imamoglu, D. D. Awschalom, G. Burkard, D. P. DiVincenzo, D. Loss, M. Sherwin, and A. Small, *Phys. Rev. Lett.* **83**, 4204 (1999); S.-B. Zheng and G.-C. Guo, *Phys. Rev. Lett.* **85**, 2392 (2000); J. I. Cirac and P. Zoller, *Nature* **404**, 579 (2000).
- [18] A. Hutton and S. Bose, *Phys. Rev. A* **69**, 042312 (2004).
- [19] N. Y. Yao, L. Jiang, A. V. Gorshkov, Z.-X. Gong, A. Zhai, L.-M. Duan, and M. D. Lukin, *Phys. Rev. Lett.* **106**, 040505 (2011); Y. Ping, B. W. Lovett, S. C. Benjamin, and E. M. Gauger, *Phys. Rev. Lett.* **110**, 100503 (2013); Y.-M. Zhu and L. Ma, *Physics Letters A* **382**, 1651 (2018); R. Grimau, A. S. Magalhães de Castro, A. Messina, and D. Valenti, *Fortschritte der Physik* **70**, 2200042 (2022).
- [20] M.-H. Yung, *Journal of Physics B: Atomic, Molecular and Optical Physics* **44**, 135504 (2011).
- [21] H.-L. Deng and X.-M. Fang, *Journal of Physics B: Atomic, Molecular and Optical Physics* **41**, 025503 (2008).
- [22] A. O. Sushkov, I. Lovchinsky, N. Chisholm, R. L. Walsworth, H. Park, and M. D. Lukin, *Phys. Rev. Lett.* **113**, 197601 (2014).
- [23] S. Haddadi, M. Ghominejad, A. Akhound, and M. R. Pourkarimi, *Scientific Reports* **11**, 22691 (2021).
- [24] D. Turkpence, F. Altintas, M. Paternostro, and Ozgur E. M ustecaplioğlu, *Europhysics Letters* **117**, 50002 (2017).
- [25] O. Arisoy and Ö. E. Müstecaplioğlu, *Scientific Reports* **11**, 12981 (2021).
- [26] J.-X. Liu, H.-L. Shi, Y.-H. Shi, X.-H. Wang, and W.-L. Yang, *Phys. Rev. B* **104**, 245418 (2021); L. Peng, W.-B. He, S. Chesi, H.-Q. Lin, and X.-W. Guan, *Phys. Rev. A* **103**, 052220 (2021).
- [27] F. Anzà, B. Militello, and A. Messina, *Journal of Physics B: Atomic, Molecular and Optical Physics* **43**, 205501 (2010); B. Militello and A. Messina, *Phys. Rev. A* **83**, 042305 (2011); X. S. Ma, G. X. Zhao, J. Y. Zhang, and A. M. Wang,

- [Quantum Information Processing](#) **12**, 321 (2013); W.-B. He, S. Chesi, H.-Q. Lin, and X.-W. Guan, [Phys. Rev. B](#) **99**, 174308 (2019); K. Karlóvá' and J. Strečka, [Molecules](#) **28** (2023), 10.3390/molecules28104037.
- [28] S. Haddadi, M. R. Pourkarimi, A. Akhound, and M. Ghominejad, [Modern Physics Letters A](#) **34**, 1950175 (2019).
- [29] C. Radhakrishnan, Z. Lü, J. Jing, and T. Byrnes, [Phys. Rev. A](#) **100**, 042333 (2019).
- [30] K. Modi, A. Brodutch, H. Cable, T. Paterek, and V. Vedral, [Rev. Mod. Phys.](#) **84**, 1655 (2012); A. Bera, T. Das, D. Sadhukhan, S. S. Roy, A. Sen(De), and U. Sen, [Reports on Progress in Physics](#) **81**, 024001 (2017).
- [31] V. E. Korepin, N. M. Bogoliubov, and A. G. Izergin, [Quantum Inverse Scattering Method and Correlation Functions](#), Cambridge Monographs on Mathematical Physics (Cambridge University Press, 1993); F. Mila, [European Journal of Physics](#) **21**, 499 (2000); T. Giamarchi, [Quantum physics in one dimension](#), International series of monographs on physics (Clarendon Press, Oxford, 2004); F. Franchini, [An Introduction to Integrable Techniques for One-Dimensional Quantum Systems](#), Lecture Notes in Physics (Springer Cham, Switzerland, 2017).
- [32] D. P. DiVincenzo, C. A. Fuchs, H. Mabuchi, J. A. Smolin, A. Thapliyal, and A. Uhlmann, [arXiv:quant-ph/9803033](#) (1998).
- [33] F. Verstraete, M. Popp, and J. I. Cirac, [Phys. Rev. Lett.](#) **92**, 027901 (2004); M. Popp, F. Verstraete, M. A. Martín-Delgado, and J. I. Cirac, [Phys. Rev. A](#) **71**, 042306 (2005).
- [34] D. Sadhukhan, S. S. Roy, A. K. Pal, D. Rakshit, A. Sen(De), and U. Sen, [Phys. Rev. A](#) **95**, 022301 (2017); J. G. Krishnan, H. K. J., and A. K. Pal, [Phys. Rev. A](#) **107**, 042411 (2023).
- [35] R. Banerjee, A. K. Pal, and A. Sen(De), [Phys. Rev. A](#) **101**, 042339 (2020); [Phys. Rev. Res.](#) **4**, 023035 (2022).
- [36] J. I. Latorre, R. Orús, E. Rico, and J. Vidal, [Phys. Rev. A](#) **71**, 064101 (2005); R. G. Unanyan, C. Ionescu, and M. Fleischhauer, [Phys. Rev. A](#) **72**, 022326 (2005).
- [37] M. B. Plenio, [Phys. Rev. Lett.](#) **95**, 090503 (2005).
- [38] A. Peres, [Phys. Rev. Lett.](#) **77**, 1413 (1996); M. Horodecki, P. Horodecki, and R. Horodecki, [Phys. Lett. A](#) **223**, 1 (1996); K. Życzkowski, P. Horodecki, A. Sanpera, and M. Lewenstein, [Phys. Rev. A](#) **58**, 883 (1998); G. Vidal and R. F. Werner, [Phys. Rev. A](#) **65**, 032314 (2002); J. Lee, M. S. Kim, Y. J. Park, and S. Lee, [Journal of Modern Optics](#) **47**, 2151 (2000).
- [39] R. H. Dicke, [Phys. Rev.](#) **93**, 99 (1954); M. Bergmann and O. Gühne, [Journal of Physics A: Mathematical and Theoretical](#) **46**, 385304 (2013); B. Lücke, J. Peise, G. Vitagliano, J. Arlt, L. Santos, G. Tóth, and C. Klempt, [Phys. Rev. Lett.](#) **112**, 155304 (2014); A. Kumar, H. S. Dhar, R. Prabhu, A. Sen(De), and U. Sen, [Physics Letters A](#) **381**, 1701 (2017).
- [40] T. J. Osborne and M. A. Nielsen, [Phys. Rev. A](#) **66**, 032110 (2002).
- [41] J. K. Stockton, J. M. Geremia, A. C. Doherty, and H. Mabuchi, [Phys. Rev. A](#) **67**, 022112 (2003).
- [42] E. Barouch, B. M. McCoy, and M. Dresden, [Phys. Rev. A](#) **2**, 1075 (1970); E. Barouch and B. M. McCoy, [Phys. Rev. A](#) **3**, 786 (1971); [Phys. Rev. A](#) **3**, 2137 (1971).
- [43] T. Chanda, T. Das, D. Sadhukhan, A. K. Pal, A. Sen(De), and U. Sen, [Phys. Rev. A](#) **94**, 042310 (2016).
- [44] C. De Dominicis and I. Giardinà, [Random Fields and Spin Glasses: A Field Theory Approach](#) (Cambridge University Press, 2006).
- [45] Y. Wang, Z. Hu, B. C. Sanders, and S. Kais, [Frontiers in Physics](#) **8** (2020), 10.3389/fphy.2020.589504.